CHIN. PHYS. LETT. Vol. 38, No. 1 (2021) 010502

Adaptive Radiative Thermal Camouflage via Synchronous Heat Conduction

Jiawei Zhang(张嘉伟)[1], Shiyao Huang(黄诗瑶)[2], and Run Hu(胡润)[2*]

[1]*Well-Tech Research Institute of China Oilfield Service Limited, Beijing 101149, China*
[2]*State Key Laboratory of Coal Combustion, School of Energy and Power Engineering, Huazhong University of Science and Technology, Wuhan 430074, China*

(Received 25 September 2020; accepted 9 November 2020; published online 6 January 2021)

The advent of transformation thermotics has seen a boom in development of thermal metamaterials with a variety of thermal functionalities, including phenomena such as thermal cloaking and camouflage. However, most thermal metamaterials-based camouflage devices only tune in-plane heat conduction, which may fail to conceal a target from out-of-plane detection. We propose an adaptive radiative thermal camouflage via tuning out-of-plane transient heat conduction, and it is validated by both simulation and experiment. The physics underlying the performance of our adaptive thermal camouflage is based on real-time synchronous heat conduction through the camouflage device and the background plate, respectively. The proposed concept and device represent a promising new approach to fabrication of conductive thermal metamaterials, providing a feasible and effective way to achieve adaptive thermal camouflage.

DOI: 10.1088/0256-307X/38/1/010502

Inspired by some amazing animals in nature, such as octopuses, squid, and chameleons, camouflage technology has witnessed great progress in recent years, exhibiting extraordinary capabilities for cloaking, concealing, camouflaging targets or creating illusions against the surrounding background in multiple frequency ranges. Of these, thermal camouflage designed with the aim of hiding/concealing objects from infrared (IR) imaging has attracted increasing attention.[1–4] Most existing thermal camouflage devices fall within the scope of a conductive regime, i.e., tuning the heat conduction in materials to create equivalent thermal temperature profiles at certain regions in order to generate the camouflage effect. Such camouflage devices are designed based on the theory of transformation thermotics or scattering cancellation techniques, resulting in a stringent requirement for anisotropic and inhomogeneous thermal metamaterials.[5–14] However, such metamaterials do not usually occur in nature, and their camouflage performance tends to deteriorate when using trade-off alternative homogeneous materials from the effective medium theory (EMT).[15–19] Although an equivalent exterior temperature profile can be achieved, the target can easily be located using an IR camera from the normal direction (z plane). Therefore, for all practical considerations, in-plane heat conduction manipulation alone is not sufficient to achieve full thermal camouflage, and alternative methods need to be explored.

According to the working principle of an IR camera, the radiation energy of a target is tuned to approximately that of the background in order to achieve thermal camouflage. Based on the Stefan–Boltzmann law, one approach is to maintain a temperature close to that of the background, and the other is to alter the surface emissivity to generate an equivalent detected temperature. Some studies, following the second strategy, have proposed radiative thermal camouflage by means of engineering surface emissivity, but a prior awareness of the background temperature is essential, which constitutes an intrinsic restriction in terms of practical applications.[20–28] Moreover, once a structure/surface with the desired emissivity has been fabricated, the radiative thermal camouflage effect can only be maintained at certain temperature distributions, and will tend to deteriorate when the temperature changes. Some studies have drawn inspiration from animal skins, such as those of cephalopods, fabricating their adaptive infrared-reflecting materials and devices under external mechanical or electrical stimuli,[29–31] but most of these cannot be manipulated automatically. In contrast, tuning the out-of-plane transient heat conduction, based on the first strategy above, has not yet been studied in detail,[32–34] and most of the resulting structures are too complicated to manufacture.

To tackle this issue, in this study we change the usual method of manipulating in-plane heat conduction in transformation thermotics, and tune the out-of-plane heat conduction to achieve adaptive thermal camouflage. Unlike in-plane thermal camouflage, the proposed out-of-plane adaptive thermal camouflage can be used to block IR detection, and could also be described as radiative thermal camouflage. We also

Supported by the National Natural Science Foundation of China (Grant No. 52076087).
*Corresponding author. Email: hurun@hust.edu.cn
© 2021 Chinese Physical Society and IOP Publishing Ltd

present a detailed mathematical deduction underpinning the design of the camouflage device, and its adaptive capability is validated both experimentally and via simulation. Further discussions regarding the fundamental mechanism and its potential applications are also presented.

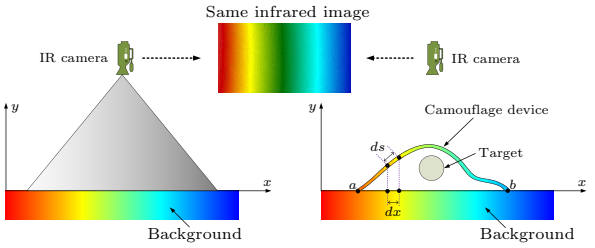

Fig. 1. Schematic of adaptive radiative camouflage device.

As shown in Fig. 1, a radiative camouflage device covers the target, and an IR camera is used to observe the temperature against a background plate. To camouflage the target, we only need to maintain the same surface temperature for the device (T_d) and background plate (T_b) from point to point in relation to the projected area of the camouflage device, i.e., $T_\mathrm{d}(x) \equiv T_\mathrm{b}(x)$, with $x \in [a, b]$, in Fig. 1(b), so that the observed IR images will mimic that shown in Fig. 1(a). As illustrated by the color gradient, when the temperatures of the device and the background within the range of $[a, b]$ are the same, the target will be concealed from the IR camera. When the space between the device and the background is large enough, the target will be concealed even when it moves inside the space. Without an additional heat source, heat conduction occurs along the background plate and the camouflage device independently in the range of $[a, b]$, as

$$\rho_i c_i \frac{\partial T_i}{\partial \tau} = \frac{\partial}{\partial x}\left(\kappa_i \frac{\partial T_i}{\partial x}\right), \tag{1}$$

where T and τ denote surface temperature and time; ρ, c, and κ denote the density, specific heat, and thermal conductivity of the device, respectively. The subscript i denotes the background plate ($i = \mathrm{b}$) and the camouflage device ($i = \mathrm{d}$). Perfect thermal camouflage performance requires $T_\mathrm{d}(x) \equiv T_\mathrm{b}(x)$ in the range of $[a, b]$ from point to point. More specifically, $T_\mathrm{b}(x)$ is the background temperature within the range of $[a, b]$ before covering the camouflage device in Fig. 1(a). For an infinitesimal segment along the background plate, the heat conduction path length is dx, while the counterpart along the camouflage device becomes the path integral of the device profile, $f(x)$, as $ds = \sqrt{1 + f'(x)^2}dx$. For the heat conduction through the background plate and the camouflage device, Eq. (1) can be rewritten as

$$\begin{aligned}
\frac{\partial T_\mathrm{b}}{\partial \tau} &= \alpha_\mathrm{b}\frac{\partial^2 T_\mathrm{b}}{\partial^2 x} + \frac{\partial \alpha_\mathrm{b}}{\partial x}\frac{\partial T_\mathrm{b}}{\partial x}, \\
\frac{\partial T_\mathrm{d}}{\partial \tau} &= \alpha_\mathrm{d}\frac{\partial^2 T_\mathrm{d}}{\partial^2 s} + \frac{\partial \alpha_\mathrm{d}}{\partial s}\frac{\partial T_\mathrm{d}}{\partial s} \\
&= \frac{\alpha_\mathrm{d}}{1 + f'(x)^2}\frac{\partial^2 T_\mathrm{d}}{\partial^2 x} \\
&\quad + \frac{\left[1 + f'(x)^2\right]\frac{\partial \alpha_\mathrm{d}}{\partial x} - \alpha_\mathrm{d} f'(x) f''(x)}{\left[1 + f'(x)^2\right]^2}\frac{\partial T_\mathrm{d}}{\partial x},
\end{aligned} \tag{2}$$

where α denotes the thermal diffusivity, $\alpha = \kappa/\rho c$. When x changes in the range of $[a, b]$, the requirement of $T_\mathrm{d}(x) = T_\mathrm{b}(x)$ only holds completely when

$$\begin{aligned}
\alpha_\mathrm{b} &= \frac{\alpha_\mathrm{d}}{1 + f'(x)^2}, \\
\frac{\partial \alpha_\mathrm{b}}{\partial x} &= \frac{\left[1 + f'(x)^2\right]\frac{\partial \alpha_\mathrm{d}}{\partial x} - \alpha_\mathrm{d} f'(x) f''(x)}{\left[1 + f'(x)^2\right]^2}.
\end{aligned} \tag{3}$$

The solution to Eq. (3) can occur only when $f'(x)f''(x) = 0$. However, $f'(x) = 0$ cannot be satisfied unless the camouflage device is completely attached to the background plate, thereby leaving no space for the target. Therefore, the reasonable solution is when $f''(x) = 0$, i.e.,

$$\begin{aligned}
f'(x) &= \tan\theta = \text{const}, \\
\alpha_\mathrm{d} &= [1 + \tan^2\theta]\alpha_\mathrm{b},
\end{aligned} \tag{4}$$

where θ is the tilt angle of the camouflage device. Since the camouflage device has to contact the background plate again at point b, we can use the piecewise linear function to describe the profile of the device. With Eq. (4), once we know the material parameters of the background plate, we can design the thermal camouflage device with repeated isosceles triangle shapes at the same tilt angle θ. The essence of this design is to achieve synchronous heat conduction throughout the camouflage device and the background plate, efficiently maintaining $T_\mathrm{d} \equiv T_\mathrm{b}$ over the whole projected area. Anything between the camouflage device and the background will consequently be thermally camouflaged in both steady or transient processes, facilitated by this adaptation to changes in background temperature. Note that adding the camouflage device to the background plate will influence the original temperature field more or less, as heat is redistributed at contact point a. However, reducing the thickness ratio of the camouflage device and the background plate will remove the influence of the original background temperature field. In this instance, we are more interested in maintaining the same temperature distribution between the camouflage device and the background plate vertically, which is the key to achieving thermal camouflage. Although the above design considers only

one-dimensional heat conduction, neglecting thermal convection and radiation, the device's performance in both simulation and experiment is confirmed below.

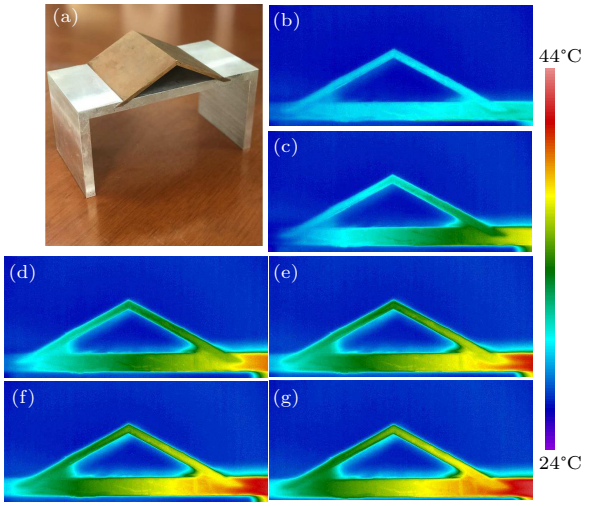

Fig. 2. Prototype of the camouflage device and temperature profiles. (a) Experimental prototype made by isosceles triangular-shaped copper and aluminum alloy 6063. Temperature profiles over time: (b) $t = 0$; (c) $t = 300$ s; (e) $t = 600$ s; (e) $t = 900$ s; (f) $t = 1200$ s; (g) $t = 1600$ s.

In order to validate our idea, as shown in Fig. 2(a), we fabricated an isosceles triangle-shaped camouflage device made of copper [$\kappa = 398\,\mathrm{W/(m{\cdot}K)}, \rho = 8930\,\mathrm{kg/m^3}$, $c = 386\,\mathrm{J/(kg{\cdot}K)}$] on a background plate made of aluminum alloy 6063 [$\kappa = 218\,\mathrm{W/(m{\cdot}K)}$, $\rho = 2690\,\mathrm{kg/m^3}$, $c = 900\,\mathrm{J/(kg{\cdot}K)}$], with a corresponding tilt angle of $\theta = 27.98°$. The thickness and width of the device are 4 mm and 100 mm, respectively, and those of the background plate are 10 mm and 100 mm. In the experiment, the background plate was set horizontally with two feet: the left foot is immersed in ice water (cold source) and the right is heated using an electric heater. In order to maintain constant surface emissivity during the infrared imaging process, both the camouflage device and the background plate were wrapped with black tape of the same thickness. An IR camera (SC620, FLIR) was used to observe the transient temperature variation at room temperature. Following calibration via a thermocouple, the surface emissivity was set at 0.9 in the IR camera, and the observed infrared images, together with elapsed time, are shown in Figs. 2(b)–2(g). We observe that heat is gradually conducted from the heat source side to the cold source side. When reaching the contact point between the device and the background plate, heat branches into two sub-paths: one is still along the background plate, and the other is along the inclined camouflage device. Qualitatively, the temperatures of the device and the plate in Fig. 2 appear to be the same at the same horizontal location. For the purpose of quantitative analysis, we extract the temperatures along the three horizontal locations, as indicated by the dashed lines 1, 2, and 3 in Fig. 3(a), and the corresponding temperatures are plotted along the length of the dashed lines in a downward direction in Fig. 3(b). Note that there are two "temperature bumps" along the curves, corresponding to the temperatures of the device and the background plate, respectively. Since the distance between the device and the background plate is longer along line 2, the distance between the two "bumps" is longer than that for the other dashed lines. Moreover, the temperatures of the two bumps are almost at the same level, as shown by the black dashed lines in Fig. 3(b), indicating the approximate temperature of the device and background plate at the same horizontal location. Outside the bumps, an ambient temperature of about 24℃ is maintained. The air temperature between the device and the background plate is relatively higher than the two ends of the dashed lines in Fig. 3(b), since the air there is heated by the experimental sample.

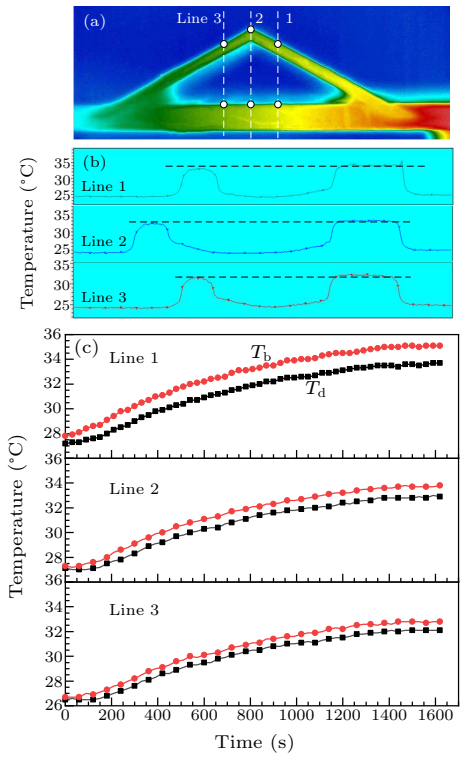

Fig. 3. Adaptive thermal camouflage with quantitative analyses. (a) Typical infrared image of the camouflage device. The three dashed lines denote the different locations, and the white dots denote the surface temperatures. (b) Temperatures along the corresponding three dashed lines in (a). (c) Surface temperature evolutions over time along the three dashed lines. The red dotted lines denote the surface temperature of the background plate, and the black squares denote the surface temperature of the camouflage device.

To explore the temperature evolution of the device and the background plate over time, as shown in Fig. 3(a), we extract the top surface temperatures of the device (T_d) and the base plate (T_b) along the three dashed lines, and plot them as shown in Fig. 3(c). It

is evident that over time, both T_d and T_b gradually increase, and that T_b is always slightly greater than T_d. The maximum temperature difference along line 1 is 1.6℃, decreasing to 0.6℃ along line 3. The reason for such a temperature deviation is twofold: (1) air convection makes some difference, particularly for the inclined device; (2) some contact thermal resistance is inevitable, leading to a small temperature difference between the device and the background plate from the beginning. In any case, the temperature between the device and the background plate at the same horizontal location is approximately the same throughout the experiment, confirming synchronous heat conduction in both the device and the background plate. Therefore, when observing downward from the normal direction (z plane), this relatively simple device is capable of achieving adaptive thermal camouflage.

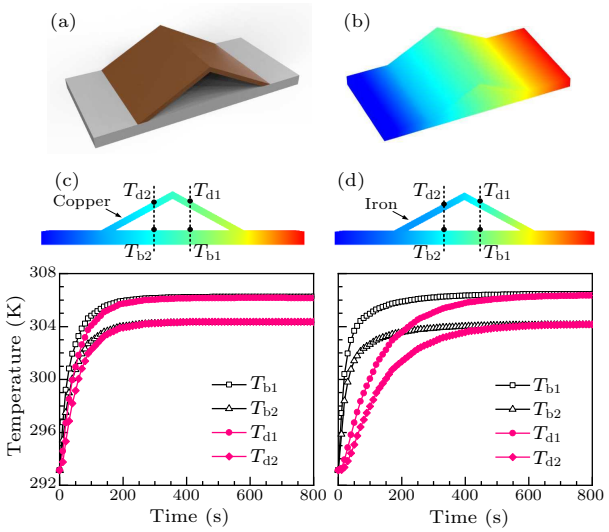

Fig. 4. (a) Schematic of the camouflage device and the background plate. (b) Simulated steady temperature field of the experimental setup. Transient temperature field comparison between (c) copper device and (d) iron device.

To further validate our explanations and ideas, we then simulated the temperature of a camouflage device with the same structure, dimensions, materials, and setup as employed in the experiments, via the finite element method (FEM), as shown in Figs. 4(a) and 4(b). Thermal contact resistance is neglected in the FEM simulations, and the air convection coefficient is set to $2\,\mathrm{W/(m^2{\cdot}K)}$, in consideration of natural convection. As shown in Fig. 3(a), we also extract and plot the surface temperatures of the camouflage device and the background plate over time at two different horizontal locations. We note that over time, T_d and T_b share the same trend, and finally reach maxima (steady state). At the same horizontal location, T_d and T_b are approximate throughout, and the maximum deviation is only about 0.1℃. Perfect synchronous heat conduction can be observed in Fig. 4(c), both qualitatively and quantitatively. Comparably, we also simulate another device with the same structure, dimension, setup, and boundary condition. Here, however we substitute the copper material with iron [$\kappa = 76.2\,\mathrm{W/(m{\cdot}K)}$, $\rho = 7870\,\mathrm{kg/m^3}$, $c = 440\,\mathrm{J/(kg{\cdot}K)}$]. Under these circumstances, the requirement condition in Eq. (4) no longer holds. Consequently, a non-negligible deviation between the curves of T_d and T_b is observed in Fig. 4(d), indicating a deterioration in the adaptive thermal camouflage effect. The curves of T_{d1} and T_{b2} overlap with the same local temperature cloud in Fig. 4(d), implying the occurrence of non-synchronous heat conduction through the camouflage device and the background plate. Based on a comparison between Figs. 4(c) and 4(d), it is proven that the proposed simple device can effectively achieve adaptive/transient thermal camouflage via synchronous heat conduction, and that Eq. (4) provides a guideline for designing such a device.

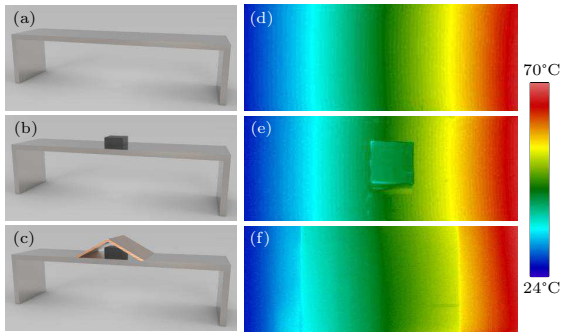

Fig. 5. Experimental radiative thermal camouflage effect. Prototypes (a)–(c) and top-view temperature profiles (d)–(f) of homogeneous background aluminum alloy plate, an object on the background plate before and after covering the copper camouflage device.

The experimental radiative thermal camouflage effect can be further observed in the top-view temperature profile comparisons shown in Fig. 5, where an object is placed in the camouflage space. The experimental prototypes and the corresponding temperature profiles are shown in Figs. 5(a)–5(c). For a homogeneous background plate [Fig. 5(a)], we observe that the temperature profile increases linearly, from the left end to the right end. When we place an object (a metal block measuring 36 mm×36 mm×16 mm) on top of the background plate [Fig. 5(b)], the temperature linearly increases with the same gradient outside the object surface. The temperature on the object's surface is much lower than that of the background plate, and has a smaller temperature gradient, which can be attributed to the low thermal conductivity of the object and the presence of contact resistance. When we cover the object with the proposed camouflage device [Fig. 5(c)], the object disappears from the top-view temperature profile, and the subsequent temperature profile is similar to that of the background plate, providing visual confirmation of the desired thermal

camouflage effect.

It should be noted that the proposed camouflage effect is achieved via synchronous heat conduction along the background plate and the isosceles triangle-shaped camouflage device. In contrast, the key point in Ref. [18] lies in point-by-point heat conduction, vertically from the background to the camouflage device, whereas our point comprises synchronous heat conduction separately along the device and the background. If the object involves heat generation, the thermal camouflage effect deteriorates in Ref. [18], whereas it can be maintained by our camouflage device if we increase the spanning distance. Although thermal convection and radiation are neglected in the deduction of the design guideline, our device's adaptive thermal camouflage performance is validated in practical applications via three-dimensional simulations and experiments. Given its real-time synchronous heat conduction, thermal camouflage is maintained adaptively, even when the background temperature changes, indicating our device's clear superiority over other thermal camouflage devices.

In conclusion, we have proposed a method of adaptive radiative thermal camouflage via tuning the out-of-plane heat conduction to achieve synchronous heat conduction. Through mathematical deduction, the basic design guideline for the radiative thermal camouflage device is obtained by achieving synchronous transient heat conduction along the background plate and the isosceles triangle-shaped camouflage device. A simple homogeneous structure is fabricated to validate the adaptive radiative camouflage performance, which is further validated via transient simulations. The proposed concept and device provide a feasible and effective way to achieve adaptive thermal camouflage, and may trigger the development of thermal metamaterials for out-of-plane heat manipulation.

References

[1] Han T C, Bai X, Thong J T L, Li B W and Qiu C W 2014 *Adv. Mater.* **26** 1731
[2] Hu R and Luo X B 2019 *Natl. Sci. Rev.* **6** 1071
[3] Liu Y, Song J, Zhao W, Ren X, Cheng Q, Luo X B, Fang N and Hu R 2020 *Nanophotonics* **9** 855
[4] Hu R, Huang S, Wang M, Luo X B, Shiomi J and Qiu C W 2019 *Adv. Mater.* **31** 1807849
[5] Song J, Huang S, Ma Y, Cheng Q, Hu R and Luo X B 2020 *Opt. Express* **28** 875
[6] Hu R, Zhou S, Li Y, Lei D Y, Luo X B, Qiu C W 2018 *Adv. Mater.* **30** 1707237
[7] Fan C Z, Gao Y and Huang J P 2008 *Appl. Phys. Lett.* **92** 251907
[8] Hu R, Huang S Y, Wang M, Zhou L L, Peng X Y and Luo X B 2018 *Phys. Rev. Appl.* **10** 054032
[9] Schittny R, Kadic M, Guenneau S and Wegener M 2013 *Phys. Rev. Lett.* **110** 195901
[10] Xu H Y, Shi X H, Gao F, Sun H D and Zhang B L 2014 *Phys. Rev. Lett.* **112** 054301
[11] Han T C, Bai X, Gao D L, Thong J T L, Li B W and Qiu C W 2014 *Phys. Rev. Lett.* **112** 054302
[12] Hu R, Liu Y, Shin S, Huang S, Ren X, Shu W, Cheng J J, Tao G, Xu W, Chen R and Luo X 2020 *Adv. Energy Mater.* **10** 1903921
[13] Ma Y G, Lan L, Jiang W, Sun F and He S L 2013 *NPG Asia Mater.* **5** e73
[14] Hu R, Wei X L, Hu J Y and Luo X B 2015 *Sci. Rep.* **4** 3600
[15] Li Y, Shen X Y, Wu Z H, Huang J Y, Chen Y X, Ni Y S and Huang J P 2015 *Phys. Rev. Lett.* **115** 195503
[16] Narayana S and Sato Y 2012 *Phys. Rev. Lett.* **108** 214303
[17] Hu R, Iwamoto S, Feng L, Ju S, Hu S, Ohnishi M, Nagai N, Hirakawa K and Shiomi J 2020 *Phys. Rev. X* **10** 021050
[18] Li Y, Bai X, Yang T, Luo H and Qiu C W 2018 *Nat. Commun.* **9** 273
[19] Li J, Li Y, Wang W, Li L and Qiu C 2020 *Opt. Express* **28** 25894
[20] Xiao L, Ma H, Liu J, Zhao W, Jia Y, Zhao Q, Liu K, Wu Y, Wei Y, Fan S and Jiang K 2015 *Nano Lett.* **15** 8365
[21] Qu Y R, Li Q, Cai L, Pan M Y, Ghosh P, Du K K and Qiu M 2018 *Light: Sci. & Appl.* **7** 26
[22] Kats M A, Blanchard R, Zhang S Y, Genevet P, Ko C, Ramanathan S and Capasso F 2013 *Phys. Rev. X* **3** 041004
[23] Coppens Z J and Valentine J G 2017 *Adv. Mater.* **29** 1701275
[24] Inoue T, De Zoysa M, Asano T and Noda S 2014 *Nat. Mater.* **13** 928
[25] Chakraborty P, Liu Y, Ma T, Guo X, Cao L, Hu R and Wang Y 2020 *ACS Appl. Mater. & Interfaces* **12** 8795
[26] Tittl A, Michel A K U, Schaferling M, Yin X H, Gholipour B, Cui L, Wuttig M, Taubner T, Neubrech F and Giessen H 2015 *Adv. Mater.* **27** 4597
[27] Salihoglu O, Uzlu H B, Yakar O, Aas S, Balci O, Kakenov N, Balci S, Olcum S, Suzer S and Kocabas C 2018 *Nano Lett.* **18** 4541
[28] Hu R, Song J, Liu Y, Xi W, Zhao Y, Yu X, Cheng Q, Tao G and Luo X 2020 *Nano Energy* **72** 104687
[29] Phan L, Kautz R, Leung E M, Naughton K L, Dyke Y V and Gorodetsky A A 2016 *Chem. Mater.* **28** 6804
[30] Phan L, IV W G W, Ordinario D D, Karshalev E, Jocson J M, Burke A M and Gorodetsky A A 2013 *Adv. Mater.* **25** 5621
[31] Xu C, Stiubianu G T and Gorodetsky A A 2018 *Science* **359** 1495
[32] Shang J, Tian B, Jiang C and Huang J 2018 *Appl. Phys. Lett.* **113** 261902
[33] Peng X and Hu R 2019 *ES Energy & Environ.* **6** 39
[34] Peng Y, Li Y, Cao P, Zhu X and Qiu C 2020 *Adv. Funct. Mater.* **30** 2002061